nature communications

Article

https://doi.org/10.1038/s41467-025-59534-3

Probing orbital magnetism of a kagome metal CsV_3Sb_5 by a tuning fork resonator

Received: 11 June 2024

Accepted: 24 April 2025

Published online: 08 May 2025

Check for updates

Hengrui Gui[1,11], Lin Yang[2,11], Xiaoyu Wang[3] ✉, Dong Chen[4,5], Zekai Shi[1], Jiawen Zhang[1], Jia Wei[1], Keyi Zhou[1], Walter Schnelle[4], Yongjun Zhang[6], Yu Liu[1], Alimamy F. Bangura[3], Ziqiang Wang[7], Claudia Felser[4], Huiqiu Yuan[1,8,9,10] ✉ & Lin Jiao[1] ✉

The recently discovered kagome metal CsV_3Sb_5 exhibits a complex phase diagram that encompasses frustrated magnetism, topological charge density wave (CDW), and superconductivity. One CDW state that breaks time-reversal symmetry was proposed in this compound, while the exact nature of the putative magnetic state remains elusive. To examine the thermodynamic state of CsV_3Sb_5 and assess the character of the associated magnetism, we conducted tuning fork resonator measurements of magnetotropic susceptibility over a broad range of angles, magnetic fields, and temperatures. We found a cascade of phase transitions in the CDW phase. Of particular interest is a highly anisotropic magnetic structure that arises below about 30 K, with a magnetic moment along the *c*-axis that has an extremely small magnitude. This magnetic state demonstrates extremely slow dynamics and small saturate field, all suggest that electronic phase below 30 K breaks time reversal symmetry and has an unconventional origin.

Materials with a kagome lattice have gathered significant research interest recently[1–3]. The interplay between band topology and electronic correlations in such systems could give rise to novel electronic phases and exotic quasiparticles[4]. AV_3Sb_5(A = K, Cs, or Rb) hosts kagome lattice of vanadium ions stacked between antimony and alkali ion layers (Fig. 1(a)). Around 80–100 K, AV_3Sb_5 exhibits a well-characterized CDW phase[5–8], followed by a series of symmetry breaking transitions upon lowering the temperature. These include rotational[9–12] or mirror[13,14] symmetry breaking, as well as superconducting phase transition[6,7]. Furthermore, a time-reversal breaking phase has been proposed based on scanning tunneling spectroscopy (STM)[13], muon spin resonance (μSR)[15,16], non-linear resistivity[17], and Kerr rotation[18] measurements, while many other groups did not find any signature of time-reversal breaking using the same probes[10–12,19,20]. However, no static magnetic moment or associated long-range magnetic order could be resolved by several advanced techniques[5,6,15,16,21,22]. Therefore, intensive debates arise regarding the nature of the low-temperature phase in AV_3Sb_5, especially in the case of CsV_3Sb_5[23], and the boundaries between different phases remain elusive.

It has been suggested that the time-reversal symmetry breaking phase in CsV_3Sb_5 is unconventional and has an orbital origin[24–32]. This phase is akin to the Haldane flux states on honeycomb lattice[33] or the loop currents in charge-transfer systems[34–36]. In the AV_3Sb_5 family, these orbital phases are currently discussed as "loop current CDW", or "CDW with loop current order"[13,15,17]. This state provides a novel origin of magnetism. What is missing is a thermodynamic signature of such

[1]Center for Correlated Matter and School of Physics, Zhejiang University, Hangzhou, China. [2]College of Materials and Environmental Engineering, Hangzhou Dianzi University, Hangzhou, China. [3]National High Magnetic Field Laboratory, Florida State University, Tallahassee, FL, USA. [4]Max Planck Institute for Chemical Physics of Solids, Dresden, Germany. [5]College of Physics, Qingdao University, Qingdao, China. [6]Hubei Key Laboratory of Photoelectric Materials and Devices, School of Materials Science and Engineering, Hubei Normal University, Huangshi, China. [7]Department of Physics, Boston College, Chestnut Hill, MA, USA. [8]Institute for Advanced Study in Physics, Zhejiang University, Hangzhou, China. [9]Institute of Fundamental and Transdisciplinary Research, Zhejiang University, Hangzhou, China. [10]State Key Laboratory of Silicon and Advanced Semiconductor Materials, Zhejiang University, Hangzhou, China. [11]These authors contributed equally: Hengrui Gui, Lin Yang. ✉e-mail: wxybkaphsc@gmail.com; hqy@zju.edu.cn; lin.jiao@zju.edu.cn

https://doi.org/10.1038/s41467-025-59534-3

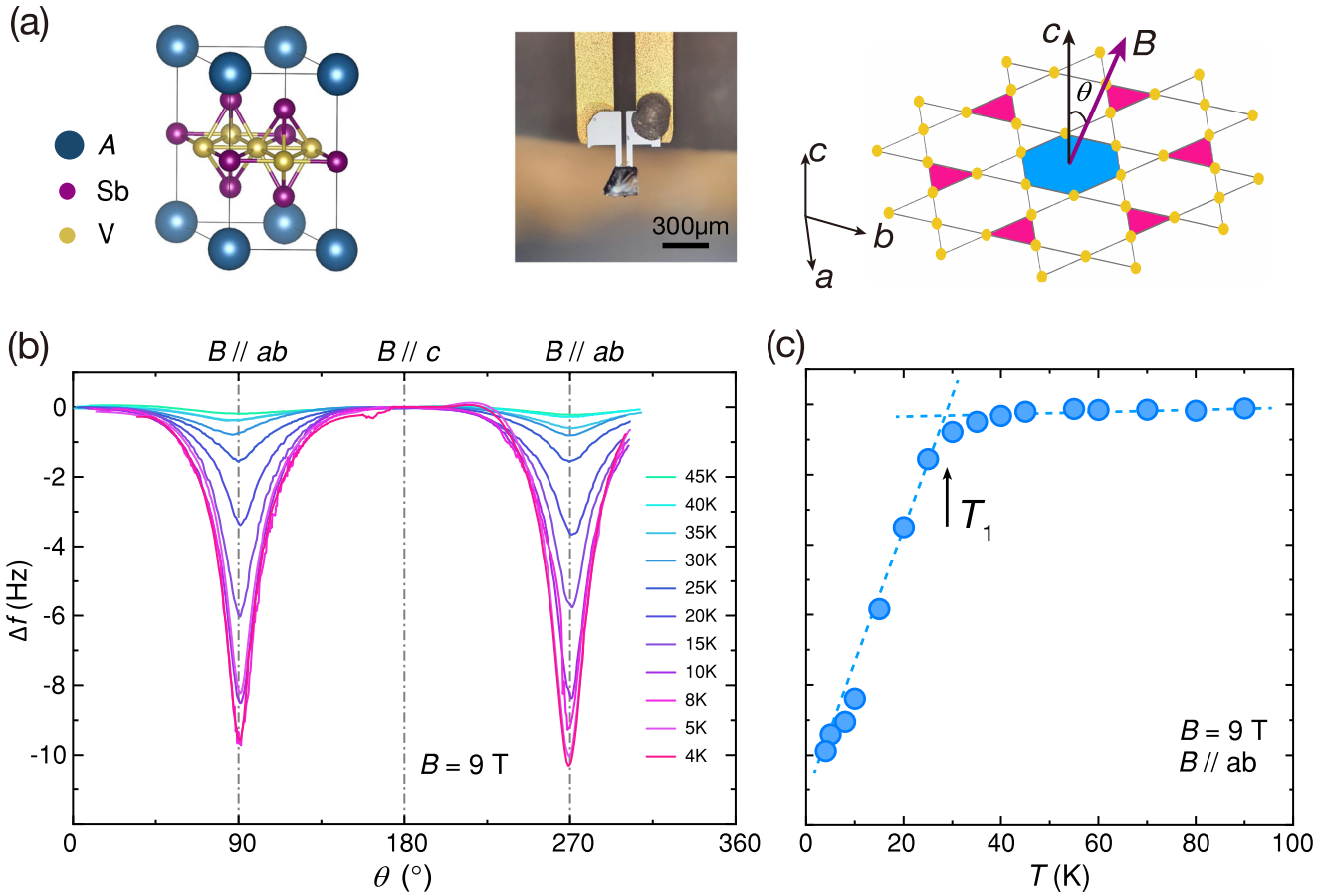

Fig. 1 | Thermodynamic phase transition across 30 K. a Crystal structure of CsV_3Sb_5. The vanadium atoms form a kagome lattice in the V-Sb1 plane which is stacked between Cs and Sb2 layers. An optical image of the 3.4 micron-thick, 300 micron-long silicon lever with a 200 × 100 × 1 micron^3 CsV_3Sb_5 crystal mounted at the tip. The sketch on the right highlights the vanadium kagome layer of CsV_3Sb_5 and defines the notation for angle θ used in the work. **b** Angular dependent relatively resonant frequency Δf measured at various temperatures with a vertical field of 9 T. Sample (#S1-1) is rotated out-of-plane at a sweep rate of $\omega_r = 0.05°/s$. **c** Averaged $\Delta f(T)$ with $\theta = 90°$ and 270°, i.e., $\mathbf{B}\|ab$.

orbital magnetism in CsV_3Sb_5. Theoretically, such orbital magnetic states can produce very small and, naturally, strongly anisotropic magnetic moments when supported by a large number of transition metal ions[35,36]. This is because orbital currents flow along adjacent sublattice, generating local moments strictly along the out-of-plane direction. In contrast, the localized spin-magnetism[37] in a 3d transition metal system (which has small spin-orbit coupling[38,39]) that tends to be weakly anisotropic. Therefore, examining the magnetism and its anisotropy is crucial for uncovering the nature of the low-temperature phase in CsV_3Sb_5.

Recently, a quartz tuning fork based technique was developed and can detect small anisotropy of susceptibility[40]. The change in the tuning fork resonant frequency Δf is directly proportional to the so-called magnetotropic susceptibility ($k(\theta)$)[41], which is defined as $k = \partial^2 F(\mathbf{B})/\partial\theta_{\mathbf{n}}^2 \propto \Delta f(\theta)$, where $\mathbf{n}$ is the axis of rotation, F is the free energy, θ is the angle between $\mathbf{B}$ and the sample (Note: we use $\mathbf{B}$ to replace $\mathbf{H}$ for convenience, as the overall susceptibility of CsV_3Sb_5 is small. See Supplementary Note 1 and Supplementary Figs. 1 and 2 for working principles of the tuning fork resonator). In this work, we show extensive tuning fork resonator measurements of the magnetotropic susceptibility in a broad temperature- and magnetic field range. Our results provide direct evidence for a small but highly anisotropic magnetic moment in CsV_3Sb_5.

Results

We studied ultra high-quality single crystals which show a very large residual resistance ratio of 300–500 (see Supplementary Fig. 3). $\Delta f(\theta)$ ($\equiv f(\theta) - f(180°)$) was measured from c-axis to the ab-plane up to 9 T, and in a temperature range from 20 mK to 110 K, see Fig. 1(b) and Supplementary Fig. 4. When the magnetic response is in the linear regime, the angular dependence of magnetotropic susceptibility follows cos(2θ) angular dependence[41]. This is consistent with our high-temperature frequency data in Fig. 1b and Supplementary Fig. 4. The tiny change of f indicates the magnetic anisotropy is negligible even at 9 T, which is in line with the metallic and paramagnetic nature of CsV_3Sb_5.

Below 30 K, Δf quickly deviates from cos(2θ) behavior and its magnitude increases dramatically (Fig. 1b). The sharp dips at 90° and 270°, i.e., $\mathbf{B}\|ab$, are signatures for extremely anisotropic magnetic moment along the c-axis, which could be nicely simulated by our simple model considering 2D ferromagnetic-type magnetic structure (see Supplementary Eq. (6) and Supplementary Fig. 5.) Theoretically, the amplitude of m is proportional to Δf between $\mathbf{B}\|ab$-plane and c-axis. In Fig. 1c, we plot the temperature dependence of $\Delta f(\theta = 90°, T)$. Indeed, the magnitude of $\Delta f(90°)$ exhibits a sharp cusp at 30 K, which increases by a factor of approximately 60 as we decrease temperature from 30 to 4 K. Such a sharp onset of the magnetotropic anisotropy

https://doi.org/10.1038/s41467-025-59534-3

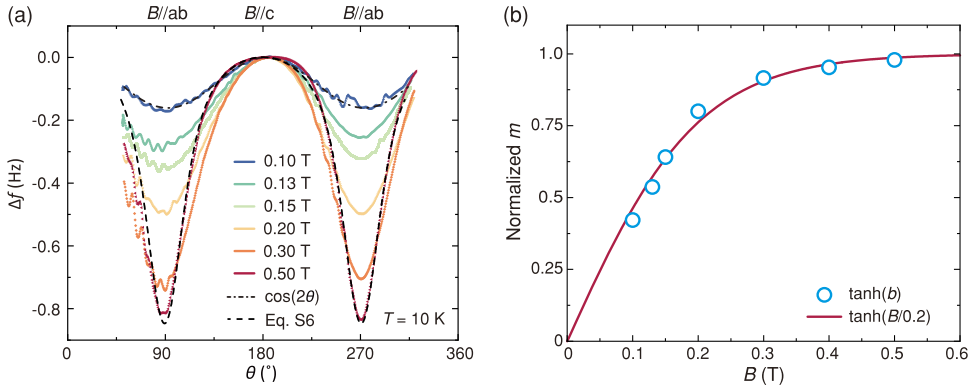

Fig. 2 | Evolution of resonant frequency at small magnetic field. a Angular dependence of the resonant frequency (sample #S2-1) at 10 K for different small magnetic fields. **b** Comparison of a hyperbolic tangent magnetization function (tanh(B/0.2), red line) and fitting parameter b in Supplementary Eq. (6) (blue circles). The three data points below 0.2 T are determined by fittings to cos(2θ) behavior, which have relatively large error bars.

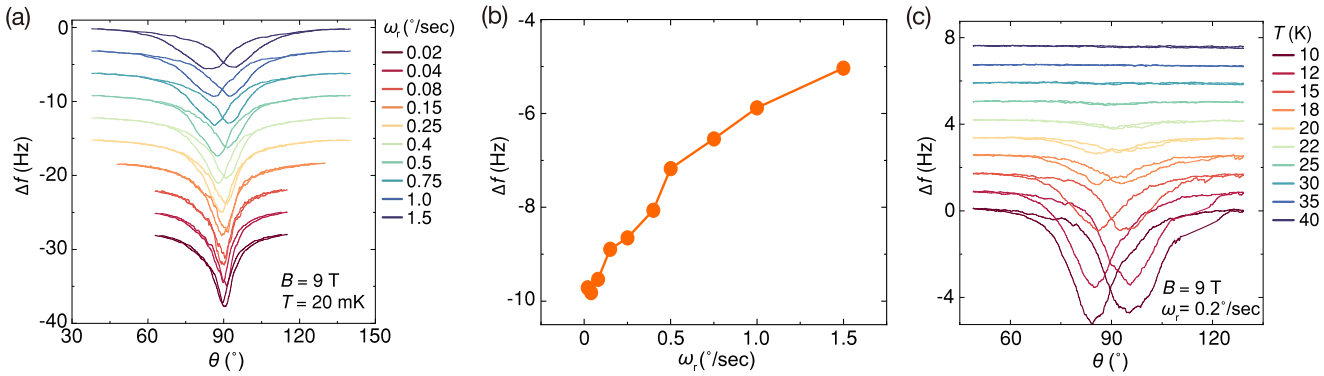

Fig. 3 | Slow dynamic of the low temperature magnetic phase. a Sweep rate (ω_r) dependent $\Delta f(\theta)$ (sample #S1-2) measured around 90° at 9 T and 20 mK. **b** (ω_r) dependent dip amplitude of $\Delta f(\theta)$ around 90°. **c** Temperature dependent $\Delta f(\theta)$ (sample #S1-1) measured in a magnetic field of 9 T, the sweep rate used here is 0.2°/sec. For clarity, curves in (**a**) and (**c**) are offset vertically along down and up direction, respectively.

below 30 K suggests a magnetic phase boundary. In this context, our measurement is very much consistent with the magnetic anomalies detected by non-linear conductivity, anomalous Nernst effect, μSR, and STM[10,15,17,42]. In fact, results from different experiments can be scaled to the same behavior which points to a thermodynamic phase boundary at 30 K, see Supplementary Fig. 6. As the measured magnetization is small along both c-axis and ab-plane (see Supplementary Figs. 7 and 8), our observations indicate the new magnetic phase possesses a small but highly anisotropic magnetic moment. We noticed that a nematic phase (rotational-symmetry-breaking phase in the ab-plane) was observed around T_1 in previous studies[10]. However, whether such an in-plane order could induce an out-of-plane magnet phase is an interesting question for further studies. In the current work, we cannot discern electronic nematicity directly.

To further investigate the novel magnetic phase, we conducted measurements on the magnetic field dependent $\Delta f(\theta)$ while maintaining the sample at 10 K. $\Delta f(\theta)$ is not only sensitive to temperature, but also shows a strong field dependence as demonstrated in Fig. 2. At a relatively high magnetic field, above 0.3 T, $\Delta f(\theta)$ shares the same lineshape as those measured at 9 T below ~30 K, see Fig. 2a. Upon reducing magnetic field, $\Delta f(\theta)$ reverts to a cos(2θ) behavior below ~0.15 T, providing evidence of the sample entering a linear regime. Figure 2b compares the normalized magnetization curve in theory (by setting B_c = 0.2 T) and the calculated m based on Supplementary Eq. (6) (with b derived from the fittings). The obtained saturate field of 0.2 T is close to the value derived from non-linear conductivity (i.e., 0.15 T)[17]. This result indicates a small external magnetic field can saturate the magnetic moment along the c-axis of CsV_3Sb_5, or induce a new magnetic phase. Recently, Guo et al., proposed that CsV_3Sb_5 possesses "correlated order at the tipping point"[23]. In such case, a small strain or magnetic field may drive the sample away from its ground state and induce symmetry-broken phases. Such an understanding is also supported by recent theoretical work[43]. The observed evolution of $\Delta f(\theta)$ curve in a small field (0.15 T) from our work is also consistent with the scenario of "correlated order at the tipping point", and time reversal symmetry breaking phase exists only above certain magnetic field.

Resonating frequency measurement also grants access to the relaxation dynamics of order parameters at very low frequencies[41]. Our measurement at ~45 kHz—a very small scale compared to exchange interactions[31] or other energy scales in CsV_3Sb_5—reveals the very slow dynamical characteristics of the magnetic phase below 30 K (Fig. 3). When ω_r < 0.15°/s, no clear hysteresis is discernible within our experimental resolution, as depicted in Fig. 3a. However, when measured at relatively high sweep rates (ω_r > 0.25°/s), the resonant frequency displays hysteretic behavior (Fig. 3a), illustrated by the splitting of the sharp dip at 90° between forward and backward sweep. Hysteresis typically emerges in magnetic materials due to time-reversal symmetry breaking together with the formation of domains. As the magnetic field rotates away from $\mathbf{B}\|ab$, the component of the magnetic field along the c-axis (B_c) increases steadily. We assume that once B_c surpass the coercive field, magnetic moments in different domains will be aligned along the external field. Our data show that, with increasing rotation

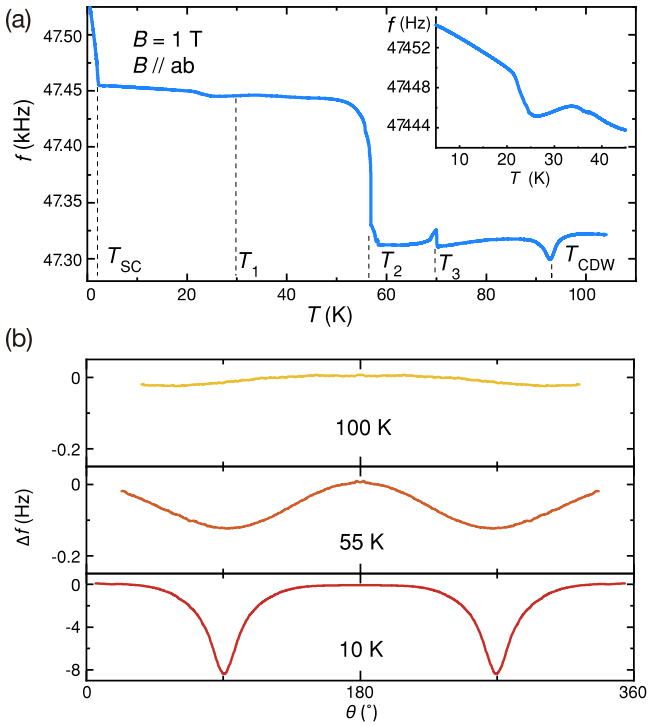

Fig. 4 | Evolution of the symmetry of the magnetotropic anisotropy. **a** Temperature dependent resonant frequency $f(T)$ (sample #S1-1) from 110 K to 2 K. Several anomalies have been detected on $f(T)$ which are denoted in the figure. Inset shows the detail of T_1 transition. **b** Angular dependent $\Delta f(\theta)$ at selected temperatures.

speed, the split dips not only further separate with each other but also experience a decrease in their magnitude (Fig. 3b). The reduced dip amplitude indicates the area between different magnetic domains tends to compensate. This hypothesis fits a picture of small domains form in CsV_3Sb_5 at low temperature, which could be aligned by an external magnetic field, as proposed by Guo et al.[17]. Remarkably, the sweep rate of 0.15°/s translates to more than 3 min between 60° and 90°, highlighting an extremely sluggish relaxation dynamics of the domains. This is in contrast to conventional spin magnetism, where the time required to flip a spin is on the order of picoseconds[44]. On the other hand, domain motion could take a long time. Once sample temperature approaching 30 K, the hysteresis behavior is invisible as shown in Fig. 3c. Again, indicating 30 K is a new magnetic phase boundary.

To probe the evolution of the CDW state and to seek the origin of the low temperature magnetic phase, we contrast the behavior of the resonant frequency across the phase boundary at 30 K and its behavior across the well-established phase boundaries at high temperatures. Figure 4a shows the resonant frequency at 1 T in the temperature range from 2 K to 100 K. In addition to a feature at T_1 = 30 K as discussed above, there is a series of anomalies being detected. Abrupt drops in the resonant frequency at 94 K and 2 K are induced by the CDW and superconducting transitions, respectively. In addition, we observed two additional anomalies: a sharp jump at 56 K, followed by a small dip at 70 K, (T_2 and T_3, respectively). The distinct jump at T_2 signifies a first-order phase transition, which is consistent with our high-resolution DC magnetization measurement, see Supplementary Figs. 3 and 8. X-ray diffraction reports a folding of the CDW superstructure along c-axis at T_2, i.e., from 2 × 2 × 4 to 2 × 2 × 2, just at T_2[45]. This suggests the 3D CDW order likely undergoes a change in its periodicity along the c-axis at T_2. T_3, however, is hardly distinguished through other transport or thermodynamic measurements. Only zero-field μSR measurements suggest the onset of a time-reversal symmetry broken phase at 70 K[15]. This measurement also identified a large signal for time-reversal symmetry breaking below T_1. While T_3 was ascribed to a development of magnetic structure on two neighboring kagome layers with the out-of-plane magnetic coupling being anti-phase. Such a configuration results in a zero moment along z-axis and much weaker magnetotropic anisotropy between T_1 and T_3. There is another possibility that the quasiparticles quickly become coherent below 30–35 K. This has been suggested from STM study as the corresponding quasiparticle interference patterns are absent above this temperature but emerge with rotation symmetry breaking below it[12]. Likely, the establishment of such coherence enhances the orbital magnetic moment and allows us to observe the magnetotropic anisotropy below T_1. This interpretation is consistent with the chiral magnetic effect observed below 30 K but not above[17]. On the other hand, if the time-reversal-symmetry breaking phase does occur above T_1 but without clear magnetic anisotropy in the ac-plane, it implies this phase is conjectured to have a three-dimensional structure, where local orbital magnetic moment contributions from adjacent layers cancel. Below T_1, different time-reversal-symmetry breaking states have been proposed (a staggered loop current ordered phase[15], striped states with a unidirectional $4a_0$ periodicity[46], or chiral nematic states[26,47].) Nevertheless, the cascade of correlated electronic states in CsV_3Sb_5 seems sensitive to sample quality and measuring environment. The high quality and small crystals used in our study might be crucial to reveal all these subtle phases.

Figure 4b encompasses typical $\Delta f(\theta)$ at selected temperatures in a magnetic field of 9 T. There is a systematic evolution of the shape of $\Delta f(\theta)$ from 2 K to 120 K. Crossing T_1, $\Delta f(\theta)$ decays from sharp dips to a $\cos(2\theta)$ behavior as shown in Fig. 1, which is a direct evidence for non-linear to linear magnetization response to the external magnetic field. Moreover, the $\cos(2\theta)$ behavior holds up to T_{CDW} (see Supplementary Fig. 4 for details), which indicates that CsV_3Sb_5 manifests itself as a paramagnetic metal with $\chi_{ab} > \chi_c$. The origin of this paramagnetic response root in the itinerant electrons which are partially gapped in the CDW phase[48]. Above T_{CDW}, $\Delta f(\theta)$ does not show any sinusoidal behavior within our experimental resolution (upper panel), therefore the sample is either isotropic or possesses an exceedingly weak susceptibility. In other words, CsV_3Sb_5 is a simple and good metal above T_{CDW}. We noticed that recent torque measurement in the ab-plane found the nematic phase even above T_{CDW}, together with evidence for time-reversal-symmetry breaking[49]. Although our torque measurement in the ac-plane detected signature for time-reversal-symmetry breaking phase below T_1 (Supplementary Fig. 9), our sample configurations (for both torque and tuning fork measurements) are not able to capture the in-plane nematic phase above[49] or below T_{CDW}[10]. Therefore, the current experiment could not exclude possible in-plane time-reversal-symmetry breaking phase at high temperature.

Discussions

In the end, we discuss the possible origin of the magnetic phase below 30 K. The magnitude of magnetotropic susceptibility provides an opportunity to estimate the magnetic moment associated with magnetic structure in CsV_3Sb_5 below 30 K. However, due to the small value of Δf and a comparable background shift below 1 T, we could not precisely derive the absolute frequency corresponding to zero field[40] for different measuring conditions. Instead, we could only provide an upper limit of $m_c \approx 0.03\,\mu_B$/vanadium ion (see Supplementary Note 2 and Supplementary Fig. 8 for details). Such a small magnetic moment is not consistent with electron-spin origin of the magnetism, and point toward orbital magnetism of itinerant electrons. It could also have been below the sensitivity limit of neutron scattering experiments[5]. We note that a recent neutron scattering study derived an upper limit of orbital magnetic moment of ~$0.02 \pm 0.01\mu_B$ per vanadium triangle[50], which is consistent with our observations. Furthermore, our thermodynamic study unveiled the formation of domains below T_1 which may

further reduce the size of the magnetic moment. With this regard, applying proper magnetic field, strain[23], or even polarized photon (which might induce electro-striction and peizomagnetic effect)[14] can further break time-reversal or lattice mirror symmetry, resulting in a single domain and detectable moment. Therefore, the small magnetic moment in our measurements is consistent with the picture of loop current CDW phase from experiments[13–18] and theories[24–29]. Such a CDW phase can be illustrated by studying the kagome lattice tight-binding model described by nearest neighbor hoppings, see Supplementary Figs. 10–12 and ref. 29 for details. The loop current order is described by a combination of real and imaginary CDWs, the latter of which breaks the time reversal symmetry. While real CDW order parameters have been shown to be the leading instability in DFT calculations[8], self-consistent Hartree–Fock studies have pointed out[26,32] that a CDW phase with both real and imaginary components can be stabilized by repulsive interactions beyond the onsite Hubbard term. Employing a simple mean-field calculation based on the LC2 state[32] (see Supplementary Section II for more details) as well as realistic estimates of the CDW order parameters lead to an orbital magnetic moment on the order of ~$0.01\mu_B$ per vanadium atom. This outcome aligns consistently with the experimentally observed small magnetic moment <$0.03\mu_B$/V-atom, without invoking domain physics. We note that the extracted orbital magnetic moment is consistent with several time-reversal-symmetry breaking CDW patterns discussed in the literature[26], and a more detailed analysis of which CDW pattern is stabilized is beyond the scope of this work.

In summary, our magnetotropic susceptibility measurements on CsV_3Sb_5 have illuminated a sequence of phase transitions below 100 K, which capture all the phase transitions reported in the literature. By closely examining the line-shape of the angular dependent resonant frequency shifts ($\Delta f(\theta)$), we established that the phase transition at around 30 K breaks time-reversal symmetry by developing an orbital magnetic moment along the *c*-axis. The orbital magnetic moment saturates to a small value at low-temperatures and above 0.2 T, consistent with an itinerant picture of magnetism due to staggered loop current. Therefore, our results provide novel insights that significantly contribute to the comprehension of AV_3Sb_5, thus shedding light on and potentially resolving several ongoing debates within this dynamic field. Moreover, our discovery uncovers a magnetic structure that goes beyond the conventional framework of spin or atomic magnetism.

Method

Sample preparation

The CsV_3Sb_5 crystals were grown by self-flux method. Cs, V, and Sb with the atonic ratio of 7:3:14 were loaded in an alumina crucible, and was subsequently sealed in a tantalum tube and a quartz tube in turn. The tube was then heated to 1000 °C, held for 20 h, and then cooled to 400 °C with a rate of 3 °C/h before the furnace was turned off. The crystals were obtained after dissolving the flux by demineralized water. Samples have been carefully characterized as shown in Supplementary Figs. 3 and 8.

Tuning fork measurement

Part of the tuning fork measurements were conducted in Quantum Design Physical Property Measurement System (PPMS) system, the rest measurements were performed in ^{3}He or dilution refrigerator systems in National High Magnetic Field Lab. The sample was placed at the tip of an Akiyama probe[51]. The resonance frequency of the probe was tracked by Zurich Instruments mid-frequency lock-in (MFLI) amplifier with the PLL/PID option. Detailed working principles and probe characterizations are included in the Supplementary Information.

Data, materials, and software availability

Relevant data generated in this study are provided in the article and Supplementary Information. All raw data that support the plots within this paper and other findings of this study are available from the corresponding authors upon request.

References

1. Ye, L. et al. Massive Dirac fermions in a ferromagnetic kagome metal. *Nature* **555**, 638–642 (2018).
2. Liu, E. et al. Giant anomalous Hall effect in a ferromagnetic kagome-lattice semimetal. *Nat. Phys.* **14**, 1125–1131 (2018).
3. Yin, J.-X. et al. Giant and anisotropic many-body spin-orbit tunability in a strongly correlated kagome magnet. *Nature* **562**, 91–95 (2018).
4. Yin, J.-X., Lian, B. & Hasan, M. Z. Topological kagome magnets and superconductors. *Nature* **612**, 647–657 (2022).
5. Ortiz, B. R. et al. New kagome prototype materials: discovery of KV_3Sb_5, RbV_3Sb_5, and CsV_3Sb_5. *Phys. Rev. Mater.* **3**, 094407 (2019).
6. Ortiz, B. R. et al. CsV_3Sb_5: A $\mathbb{Z}_2$ topological kagome metal with a superconducting ground state. *Phys. Rev. Lett.* **125**, 247002 (2020).
7. Yin, Q. et al. Superconductivity and normal-state properties of kagome metal RbV3Sb5 single crystals. *Chin. Phys. Lett.* **38**, 037403 (2021).
8. Tan, H., Liu, Y., Wang, Z. & Yan, B. Charge density waves and electronic properties of superconducting kagome metals. *Phys. Rev. Lett.* **127**, 046401 (2021).
9. Xiang, Y. et al. Twofold symmetry of c-axis resistivity in topological kagome superconductor CsV_3Sb_5 with in-plane rotating magnetic field. *Nat. Commun.* **12**, 6727 (2021).
10. Nie, L. et al. Charge-density-wave-driven electronic nematicity in a kagome superconductor. *Nature* **604**, 59–64 (2022).
11. Li, H. et al. Rotation symmetry breaking in the normal state of a kagome superconductor KV_3Sb_5. *Nat. Phys.* **18**, 265–270 (2022).
12. Li, H. et al. Unidirectional coherent quasiparticles in the high-temperature rotational symmetry broken phase of AV_3Sb_5 kagome superconductors. *Nat. Phys.* **19**, 637–643 (2023).
13. Jiang, Y.-X. et al. Unconventional chiral charge order in kagome superconductor KV_3Sb_5. *Nat. Mater.* **20**, 1353–1357 (2021).
14. Xing, Y. et al. Optical manipulation of the charge-density-wave state in RbV3Sb5. *Nature* **631**, 60–66 (2024).
15. Yu, L. et al. Evidence of a hidden flux phase in the topological kagome metal CsV_3Sb_5. *arXiv2107.10714* (2021).
16. Mielke, C. et al. Time-reversal symmetry-breaking charge order in a kagome superconductor. *Nature* **602**, 245–250 (2022).
17. Guo, C. et al. Switchable chiral transport in charge-ordered kagome metal CsV_3Sb_5. *Nature* **611**, 461–466 (2022).
18. Xu, Y. et al. Three-state nematicity and magneto-optical kerr effect in the charge density waves in kagome superconductors. *Nat. Phys.* **18**, 1470–1475 (2022).
19. Li, H. et al. No observation of chiral flux current in the topological kagome metal CsV_3Sb_5. *Phys. Rev. B* **105**, 045102 (2022).
20. Saykin, D. R. et al. High resolution polar kerr effect studies of CsV_3Sb_5: Tests for time-reversal symmetry breaking below the charge-order transition. *Phys. Rev. Lett.* **131**, 016901 (2023).
21. Kenney, E. M., Ortiz, B. R., Wang, C., Wilson, S. D. & Graf, M. J. Absence of local moments in the kagome metal KV_3Sb_5 as determined by muon spin spectroscopy. *J. Phys.: Condens. Matter* **33**, 235801 (2021).
22. Shan, Z. et al. Muon spin relaxation study of the layered kagome superconductor CsV_3Sb_5. *Phys. Rev. Res.* **4**, 033145 (2022).
23. Guo, C. et al. Correlated order at the tipping point in the kagome metal CsV3Sb5. *Nat. Phys.* **20**, 579–584 (2024).
24. Feng, X., Jiang, K., Wang, Z. & Hu, J. Chiral flux phase in the kagome superconductor AV_3Sb_5. *Sci. Bull.* **66**, 1384–1388 (2021).

25. Park, T., Ye, M. & Balents, L. Electronic instabilities of kagome metals: saddle points and landau theory. *Phys. Rev. B* **104**, 035142 (2021).
26. Denner, M. M., Thomale, R. & Neupert, T. Analysis of charge order in the kagome metal AV_3Sb_5 (*A* = K, Rb, Cs). *Phys. Rev. Lett.* **127**, 217601 (2021).
27. Lin, Y.-P. & Nandkishore, R. M. Complex charge density waves at Van Hove singularity on hexagonal lattices: Haldane-model phase diagram and potential realization in the kagome metals AV_3Sb_5 (*A* = K, Rb, Cs). *Phys. Rev. B* **104**, 045122 (2021).
28. Feng, X., Zhang, Y., Jiang, K. & Hu, J. Low-energy effective theory and symmetry classification of flux phases on the kagome lattice. *Phys. Rev. B* **104**, 165136 (2021).
29. Zhou, S. & Wang, Z. Chern fermi pocket, topological pair density wave, and charge-4e and charge-6e superconductivity in kagome superconductors. *Nat. Commun.* **13**, 7288 (2022).
30. Christensen, M. H., Birol, T., Andersen, B. M. & Fernandes, R. M. Loop currents in AV_3Sb_5 kagome metals: Multipolar and toroidal magnetic orders. *Phys. Rev. B* **106**, 144504 (2022).
31. Tazai, R., Yamakawa, Y., Onari, S. & Kontani, H. Mechanism of exotic density-wave and beyond-Migdal unconventional superconductivity in kagome metal AV3Sb5 (A = K, Rb, Cs). *Sci. Adv.* **8**, eabl4108 (2022).
32. Dong, J.-W., Wang, Z. & Zhou, S. Loop-current charge density wave driven by long-range coulomb repulsion on the kagomé lattice. *Phys. Rev. B* **107**, 045127 (2023).
33. Haldane, F. D. M. Model for a quantum hall effect without landau levels: condensed-matter realization of the "parity anomaly". *Phys. Rev. Lett.* **61**, 2015–2018 (1988).
34. Varma, C. M. & Giamarchi, T. *Strongly Interacting Fermions and High T_c Superconductivity* (Proceedings of the Les Houches Summer School of Theoretical Physics, Les Houches, 1991, edited by B. Doucot and J. Zinn-Justin, Session LVI (Elsevier, 1995).
35. Varma, C. M. Non-fermi-liquid states and pairing instability of a general model of copper oxide metals. *Phys. Rev. B* **55**, 14554–14580 (1997).
36. Shekhter, A. & Varma, C. M. Local magnetic moments due to loop currents in metals. *Phys. Rev. B* **106**, 214419 (2022).
37. Anderson, P. W. Localized magnetic states in metals. *Phys. Rev.* **124**, 41–53 (1961).
38. Rad, G. T. *Magnetism,* edited by H. Suhl (Academic Press, 2012).
39. Greenwood, N. N. & Earnshaw, A. *Chemistry of the Elements (2nd ed.)* (Elsevier, 1985).
40. Modic, K. A. et al. Scale-invariant magnetic anisotropy in $RuCl_3$ at high magnetic fields. *Nat. Phys.* **17**, 240–244 (2021).
41. Shekhter, A., McDonald, R. D., Ramshaw, B. J. & Modic, K. A. Magnetotropic susceptibility. *Phys. Rev. B* **108**, 035111 (2023).
42. Chen, D. et al. Anomalous thermoelectric effects and quantum oscillations in the kagome metal CsV_3Sb_5. *Phys. Rev. B* **105**, L201109 (2022).
43. Tazai, R., Yamakawa, Y. & Kontani, H. Drastic magnetic-field-induced chiral current order and emergent current-bond-field interplay in kagome metals. *Proc. Natl Acad. Sci.* **121**, e2303476121 (2024).
44. de la Torre, A. et al. Colloquium: nonthermal pathways to ultrafast control in quantum materials. *Rev. Mod. Phys.* **93**, 041002 (2021).
45. Stahl, Q. et al. Temperature-driven reorganization of electronic order in CsV_3Sb_5. *Phys. Rev. B* **105**, 195136 (2022).
46. Zhao, H. et al. Cascade of correlated electron states in the kagome superconductor CsV_3Sb_5. *Nature* **599**, 216–221 (2021).
47. Grandi, F., Consiglio, A., Sentef, M. A., Thomale, R. & Kennes, D. M. Theory of nematic charge orders in kagome metals. *Phys. Rev. B* **107**, 155131 (2023).
48. Gruner, G. *Density Waves in Solids* ((Addison-Wesley, 1994).
49. Asaba, T. et al. Evidence for an odd-parity nematic phase above the charge-density-wave transition in a kagome metal. *Nat. Phys.* **20**, 40–46 (2024).
50. Liège, W. et al. Search for orbital magnetism in the kagome superconductor CsV_3Sb_5 using neutron diffraction. *Phys. Rev. B* **110**, 195109 (2024).
51. Akiyama, T. et al. Implementation and characterization of a quartz tuning fork based probe consisted of discrete resonators for dynamic mode atomic force microscopy. *Rev. Sci. Instrum.* **81**, 063706 (2010).

Acknowledgements

The authors thank Arkady Shekhter for his substantial help in data analysis and writing the manuscript. Work at Zhejiang University was supported by the National Key R&D Program of China (Grant Nos. 2023YFA1406100 and 2022YFA1402200), the Zhejiang Provincial Natural Science Foundation of China (Grant No. LR25A040003), the Fundamental Research Funds for the Central Universities (Grants Nos. 226-2024-00039 and 226-2024-00068), and the National Natural Science Foundation of China (Grants Nos. 12374151, 12034017, and 12350710785). Measurements performed at the National High Magnetic Field Laboratory are supported by the National Science Foundation Cooperative Agreement (No. DMR-2128556, No. DMR-1644779) and the State of Florida. Z.W. is supported by the US DOE, Basic Energy Sciences Grant No. DE-FG02-99ER45747 and SEED Award No. 27856 from Research Corporation for Science Advancement. C.F., W.S., and D.C.'s work at MPI-CPfS is supported by Deutsche Forschungsgemeinschaft (DFG) under SFB1143 (Project No. 247310070), the European Research Council Advanced Grant (No. 742068) "TOPMAT," and the DFG through the Würzburg-Dresden Cluster of Excellence on Complexity and Topology in Quantum Matter ct.qmat (EXC 2147, Project-ID No. 39085490).

Author contributions

L.J., X.W., and H.Y. conceived the project. H.G., L.Y., Z.S., J.W., K.Z., and A.B. performed experimental measurements. D.C., W.S., and C.F. provided CsV_3Sb_5. J.Z., Y.L., and Y.Z. provided samples for control experiments. X.W., and Z.W. performed theoretical analysis. L.J. and X.W. wrote the manuscript with the input of all authors.

Competing interests

The authors declare no competing interests.

Additional information

Supplementary information The online version contains supplementary material available at https://doi.org/10.1038/s41467-025-59534-3.

Correspondence and requests for materials should be addressed to Xiaoyu Wang, Huiqiu Yuan or Lin Jiao.

Peer review information *Nature Communications* thanks Jia-Xin Yin, and the other, anonymous, reviewers for their contribution to the peer review of this work. A peer review file is available.